Desalination and Water Treatment
www.deswater.com

doi: 10.5004/dwt.2017.21444

90 (2017) 168–179
September

Numerical investigation and optimization for performance analysis in Venturi inlet cyclone separator

S. Venkatesh[a,*], M. Sakthivel[b]

[a]*Mechanical Engineering, Sri Eshwar College of Engineering, Coimbatore, Tamil Nadu, India, email: venkatesme2014@gmail.com*
[b]*Mechanical Engineering, Anna University Regional Campus, Coimbatore, Tamil Nadu, India, email: sakthi_vel_m@yahoo.com*

Received 17 May 2017; Accepted 12 September 2017

ABSTRACT

A mathematical model has been developed for Venturi inlet cyclone separator by considering various geometric parameters. The most important geometrical parameters such as Venturi inlet length and Venturi inlet width and outlet diameter are considered for optimization. Response surface methodology has been used to fit the quadratic polynomial equation and the significance of quadratic model is tested by using analysis of variance. These parameters are optimized to get minimum pressure drop in cyclone separator by means of genetic algorithm. The optimized new design gives less pressure drop and high collection efficiency compared with mathematical model. The Reynolds stress turbulence model and discrete phase model have been utilized to simulate the Venturi inlet cyclone separator. The results from optimized design such as pressure drop, cut-off diameter, Euler number and Stokes number were compared with the results of computational fluid dynamics technique and found highly agreeing.

Keywords: Mathematical model; Pressure drop; Response surface methodology; Genetic algorithm; Reynolds stress model; Discrete phase model

1. Introduction

Industries related to chemical engineering, mineral processing and foundry processing, etc., are more prone to environmental issues as the process involved creates hazardous impacts to the environment with higher consumption of energy. To minimize the hazardous impact on the environment different strategies have been followed rigorously, such as cyclone separators, electrostatic precipitators, etc. [1]. Cyclone separator is primary dust collecting equipment for removing particulates from fluid medium. The removal of particulates in this process is usually carried out without the aid of filters by the action of vortex separation. The effectiveness of the segregation of particulates depends upon the geometrical parameters of the cyclone separator and pressure drop. It is worthy to note that the higher pressure drop, lower the efficiency of the particulates segregation and higher the operating power [2]. Due to higher pressure drop, the particulates which can be segregated escape out of the cyclone separator. The escaped particulates are further subjected to the secondary purification process. In this stage, higher water resource, energy and recycling time are involved [3]. This makes it mandatory to provide with optimized geometrical constraints for the separator to create necessary pressure drop which induces the maximum segregation of particulates inside the separator thereby minimizing the energy resources required in the secondary purification process.

Many researchers used different approaches to improve the performance of cyclone. Xu et al. [4] utilized the slotted form vortex finder to develop the performance of cyclone. Also, Gu et al. [5] utilized a pressure transducer to assess the pressure at dissimilar locations for performance study. Besides, the performance of the cyclone separator has been examined with different dust outlet geometries [6]. In addition, the performance has been assessed with various inlet patterns such as single normal inlet, double normal inlet and double declining inlet [7]. Also, Bernardo et al. [8] used a scroll inlet duct in the cyclone body to describe the gas and

* Corresponding author.

gas solid flow in a cyclone. Adjusting the cone tip diameter also increases the collection efficiency and decreases the pressure drop [9]. In addition, a novel exhaust under different insert depths and sloping orientations has been used to improve the performance [10]. Gong et al. [11] studied the internal flow field by using different helix angle in the cyclone. Adjusting the vortex finder shape and size gives a good result on the cyclone performance [12]. To improve the cyclone performance, many researchers follow some technical approaches such as optimization techniques and extra devices added with cyclone separator. Optimization techniques such as multiobjective optimization and genetic algorithm (GA) have been used to change the existing geometric constraints of the cyclone [13,14]. Extra devices such as a post-cyclone have been positioned above the vortex finder to collect the escaping particles [15]. A rotational classifier has been fixed instead of the vortex finder in a dynamic cyclone to improve the performance [16].

In this research, a vertical Venturi inlet has been added with tangential inlet of the cyclone separator. The Venturi has three sections such as convergent, throat and divergent section. Initially the particles are admitted with high velocity in convergent section. When the particles are entering through the divergent section, the velocity of the particles is reduced. The particles entering with less velocity into the cyclone separator cannot easily escape to the atmosphere. In addition, the industries such as foundry and steel plants also used Venturi type scrubbers to capture the flying dust particles. Therefore, in this research a Venturi inlet has been used to improve the performance of cyclone separator. At first, a mathematical model has been formed. The pressure drop, cut-off diameter, Euler number and Stokes number of this mathematical model have been predicted mathematically. Then, this model has been optimized by response surface methodology (RSM) and GA. These optimized results are simulated in computational fluid dynamics (CFD) software (Ansys Fluent). In CFD, the Reynolds stress turbulence model (RSTM) and discrete phase model (DPM) have been used for the simulation.

2. Mathematical model

Several researchers created theoretical and physical models in the past decades such as Stairmand model [17], Avci and Karagoz model [18], Muschelknautz model [19], Chen and Shi model [20] and Zhao model [21]. In this research, Shepherd and Lapple [22] model has been used to set the initial mathematical model of the cyclone separator. Furthermore, a Venturi inlet has been added at the tangential inlet of the cyclone. The schematic diagram of Venturi inlet cyclone separator and its geometric features are shown in Fig. 1 and Table 1. In this model, the particles are entering through a Venturi inlet then it is entered through the tangential entry of the cyclone separator. Now the particles are swirling around the vortex finder region due to centrifugal force. After that, it is gradually settled at the bottom of the cyclone separator and gas exits through the outlet tube.

2.1. Pressure drop and cut-off diameter

Estimating the pressure drop and cut-off diameter is an important one because these boundaries, decide the performance of the cyclone. The pressure drop and cut-off diameter of the mathematical model have been estimated by Eqs. (1) and (3) [22]. The dimensionless pressure drop or Euler number has been predicted with the help of Eq. (4). The number of turns has been calculated by Eq. (5). The Stokes number based on cut-off diameter has been determined by Eq. (6) [23]. The required parameters to calculate the pressure drop, cut-off diameter, Euler number, number of turns and Stokes number are given in Tables 1 and 2. The estimated pressure drop (Δp) for this mathematical model cyclone is 895.8 N/m^2 at velocity 5 m/s. The predicted cut-off diameter (X_{50}) is 1.85×10^{-5} m at a velocity of 1 m/s. The head and number of turns have been evaluated by Eqs. (2) and (5). The value of head and number of turns are 58.5 and 2.4, respectively. The calculated dimensionless Euler number (E_u) is 58.54 at a velocity of 5 m/s and Stokes number (Stk_{50}) is 0.021364 at a velocity of 1 m/s. The following equations are used to find the abovesaid parameters.

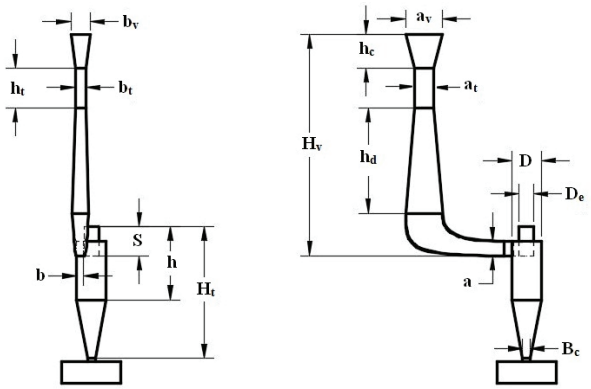

Fig. 1. Layout diagram of Venturi inlet cyclone separator.

Table 1
Dimensional parameters of the Venturi inlet cyclone separator

S.No.	Parameters	Dimension (mm)
1	Cyclone diameter (D)	100
2	Inlet height (a)	50
3	Inlet width (b)	25
4	Outlet diameter (D_e)	50
5	Total height (H_t)	400
6	Body height (h)	200
7	Cone tip diameter (B_c)	25
8	Outlet length (S)	62.5
9	Venturi inlet length (a_v)	125
10	Venturi inlet width (b_v)	65
11	Height of convergent section (h_c)	115
12	Height of divergent section (h_d)	360
13	Height of throat section (h_t)	135
14	Venturi throat length (a_t)	65
15	Venturi throat width (b_t)	35
16	Total height of the Venturi (H_v)	755

Table 2
Input parameters

S.No.	Input parameters	Values
1	Particle density (ρ_p), kg/m^3	2,000
2	Inlet velocity (V_i), m/s	5
3	Gas density (ρ_g), kg/m^3	1.225
4	Viscosity (μ), kg/ms	1.78×10^{-5}
5	Venturi inlet length (a_v), m	0.125
6	Venturi inlet width (b_v), m	0.065
7	Gas outlet diameter (D_e), m	0.050
8	Number of turns (N_e)	2.4

$$\text{Pressure drop } (\Delta p) = 0.5\rho_g V_i^2 H_v \tag{1}$$

$$\text{Head } (H_d) = \frac{Kab}{D_e^2} \tag{2}$$

where $K = 18$ is a constant.

$$\text{Cut-off diameter } (X_{50}) = \left[\frac{9\mu b_v}{2\pi N_e V_i(\rho_p - \rho_g)}\right]^{0.5} \tag{3}$$

$$\text{Euler number } (E_u) = \frac{\Delta p}{0.5\rho_g V_i^2} \tag{4}$$

$$\text{Number of turns } N_e = \frac{1}{a}\left[h + \frac{H_t - h}{2}\right] \tag{5}$$

$$\text{Stokes number } (\text{Stk}_{50}) = \frac{\rho_p X_{50}^2 V_i}{18\mu D} \tag{6}$$

3. Response surface methodology

In the previous section, pressure drop and cut-off diameter of the given mathematical model have been found. In order to improve the performance, the pressure drop must decrease without affecting the efficiency of the cyclone. According to the literature survey, three parameters are mostly affecting the performance of the cyclone. The three parameters are inlet height, inlet width and outlet diameter [24]. In this study, Venturi equipment has been added with a cyclone separator; hence, inlet length (a_v) and inlet width (b_v) of the Venturi and outlet diameter (D_e) of the cyclone have been selected for optimization. Usually, optimization of any experimental setup is based on adjusting one parameter and keeping all others as constant. This procedure has been followed until optimum values are found. It is a time-consuming process. Also, it cannot give an interaction result with response parameters for a complex system. Moreover, a multivariate parametric study has to be conducted for explaining response and interactions of several complicated schemes [25]. In this study, RSM has been used. It is a good technique for solving multivariate problems. The RSM was introduced by Box and Wilson [26]. Recently, this method is mostly used in process optimization in the field of engineering and manufacturing. Consecutively to perform an RSM analysis, the first one has to classify the experimental parameters and the response parameter. Based on this classification, the experiment has been designed. After this initial process, the data have been tabulated by conducting the experiment. Then, the second-order polynomial equation has been fit based on this experimental data [25]. The global quadratic model used in the response surface analysis is as follows:

$$Y = \beta_o + \sum_{i=j}^{7}\beta_i X_i + \sum_{i=j}^{7}\beta_{ii} X_i^2 + \sum\sum_{i<j}\beta_{ij} X_i X_j \tag{7}$$

3.1. Design of experiment

In this work, the Minitab software has been used to fitting the regression equation by RSM. In this method, Box–Behnken design (BBD) has been selected and number of factors and number of runs have been selected as 3 and 15, respectively. At first, for creating the response surface design the minimum and maximum values of three important geometric parameter values such as Venturi inlet length, Venturi inlet width and outlet diameter of the cyclone have been given in the factors input table. There are two levels: the first level has a minimum value of three parameters and the second level has a maximum value of three parameters which is shown in Table 3. After feeding the data in level factors table, then the BBD matrix has been produced with actual variables for 15 runs. The response parameter such as pressure drop has been calculated for the created 15 runs. These 15 pressure drop values have been determined mathematically with the help of Eqs. (1) and (2). The BBD matrix with pressure drop values is shown in Table 4. After that, this response surface design has been analyzed for forming the regression coefficient with 95% of the confidence level ($P < 0.05$) for all tests. The R^2 value of the model is 0.9993 which is very close to 1. Hence, it suggests that the model is very effective. Also, the predicted R^2 value is 0.9886 and adjusted R^2 value is 0.998. Both these values are nearly equal, so it gives a good agreement between them. In this analysis, the surface plots such as pressure drop vs. Venturi inlet length and Venturi inlet width; pressure drop vs. Venturi inlet length and cyclone outlet diameter; pressure drop vs. Venturi inlet width and cyclone outlet diameter have been plotted which is shown

Table 3
Two levels of the factors

S.No.	Geometric ratios	Low (mm)	High (mm)
1	Venturi inlet length (a_v)	100	130
2	Venturi inlet width (b_v)	40	70
3	Outlet diameter (D_e)	50	70

Table 4
BBD matrix with actual variables and pressure drop values

S.No.	Venturi inlet length (a_v), mm	Venturi inlet width (b_v), mm	Outlet diameter ratio (D_e), mm	Pressure drop (Δp), N/m^2
1	100	40	60	306.3
2	130	40	60	398.1
3	100	70	60	535.9
4	130	70	60	696.7
5	100	55	50	606.4
6	130	55	50	788.3
7	100	55	70	309.4
8	130	55	70	402.2
9	115	40	50	507.1
10	115	70	50	887.5
11	115	40	70	258.8
12	115	68	68	466.1
13	115	54	58	508.8
14	115	53	56	535.7
15	115	52	54	565.2

in Fig. 2. The created regression equation or second-order polynomial model is as follows:

$$Z = 538.076 + 7.599 \times a_v + 19.086 \times b_v - 33.653 \times D_e + 0.006 \times a_v^2 + 0.003 \times b_v^2 + 0.426 \times D_e^2 + 0.077 \times a_v \times b_v - 0.148 \times a_v \times D_e - 0.317 \times b_v \times D_e \quad (8)$$

3.2. Analysis of variance

For conducting the F test on the individual variables and interactions, analysis of variance (ANOVA) has been followed in this study. ANOVA has been used to estimate significance of the created quadric polynomial model. This test suggests that the maximum value of F ratio gives more significant effect on respective parameters. It means the P value is small ($P < 0.05$) when the F ratio is high. If F ratio is low, then the P value is high ($P > 0.05$) and it points out the most insignificant parameters in the quadric model. Table 5 shows the results of ANOVA for the given quadric polynomial model. The identified results are as follows. The F value is the maximum for Venturi inlet width and outlet diameter ($P < 0.05$) in linear terms. So these two response variables are more significant. The Venturi inlet length has insignificant effect because the F value is low ($P > 0.05$). Further, in quadric terms outlet diameter gives more significant effect compared with other two parameters. However, the interaction between the Venturi inlet length and Venturi inlet width, Venturi inlet length and outlet diameter, and Venturi inlet width and outlet diameter gives more significant effect with 95% of the confidence level ($P < 0.05$).

From surface plot (a) one can easily identify that the pressure drop increases when increasing the inlet length and inlet width of the Venturi. Furthermore, decreasing these two values gives less pressure drop. In addition, the surface plot (b) has given results such as increasing the outlet diameter produces a low-pressure drop and increasing the inlet length creates a high-pressure drop. Also, surface plot (c) has given results such as increasing the outlet diameter produces a low-pressure drop and increasing the inlet width creates a high-pressure drop. These three surface plots show that the inlet length and inlet width must be decreased for decreasing the pressure drop and at the same time outlet diameter must be increased for decreasing the pressure drop. However, decreasing the inlet length and inlet width gives less collection efficiency. Because of this reason an optimized parameter value is needed to increase the collection efficiency and decrease the pressure drop. Therefore, in this study the generated second-order polynomial model is to be optimized by GA.

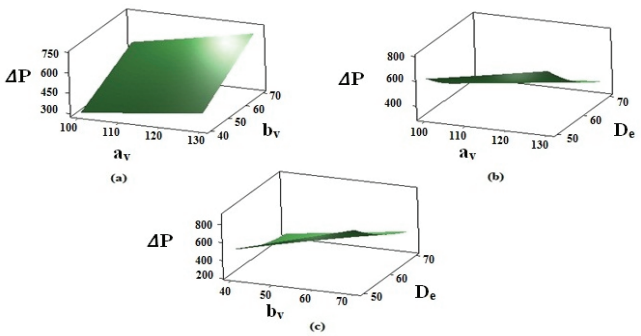

Fig. 2. Surface plots of (a) pressure drop vs. Venturi inlet length and inlet width, (b) pressure drop vs. Venturi inlet length and outlet diameter and (c) pressure drop vs. inlet width and outlet diameter.

4. Genetic algorithm

GA is a non-traditional optimization technology. It was invented by John Holland in 1960. It is an arbitrary search algorithm that models a process of developing population individuals. Nowadays, GA is used in product design, machine design and manufacturing processes to attain the best solutions. Usually, it begins with a set of solutions and varying them through several iterations. Also, it converges to

the most-fit solution by this iteration. It has three basic operators such as selection or reproduction operator, crossover operator and mutation operators. Selection is the phase of GA in which individual genomes have been preferred from population intended for afterward reproduction. There are seven selection processes available such as the roulette wheel selection, Boltzmann selection, rank selection, tournament selection, steady-state selection, sigma selection and elitism. The role of the crossover is dividing two chromosomes and then uniting one half of every chromosome with another pair. There are four types such as single-point, two-point, uniform and arithmetic crossover. Mutation engages with a single bit of a chromosome. The chromosomes are assessed under some fitness criteria. After evaluation, the best one is kept and others are discarded. There are four types of mutation such as Gaussian, uniform, adaptive feasible and custom [27,28]. Currently, MATLAB software is mostly used in optimization. It gives high performance numerical calculation and visualization. In this study, MATLAB software has been used to find the best optimized solution from GA.

4.1. Genetic algorithm settings in MATLAB

Before commencing the optimization in MATLAB, the mathematical model equation has been set by design of experimental technique. In this study, the polynomial quadric equation has been created by RSM which is given in Eq. (8). From this mathematical model, the objective function has been developed which is given in Eq. (9). In addition, the objective function is used to create the fitness function. In order to perform the optimization with MATLAB, an m-file has been created in notepad for fitness function. In this file, the fitness function is clearly written based on Eq. (9). In this equation, S(1), S(2) and S(3) are corresponding to Venturi inlet length (a_v), Venturi inlet width (b_v) and cyclone outlet diameter (D_e). The created m-file fitness function is as follows:

Function Z = f(S)

$$Z = 538.076 + 7.599 \times S(1) + 19.086 \times S(2) - 33.653 \times S(3) + 0.006 \times S(1) \times S(1) + 0.003 \times S(2) \times S(2) + 0.426 \times S(3) \times S(3) + 0.077 \times S(1) \times S(2) - 0.148 \times S(1) \times S(3) - 0.317 \times S(2) \times S(3) \quad (9)$$

After saving the m-file, the GA settings are mentioned by opening the GA window. At first, the fitness function and a number of variables are mentioned in the GA window. Population type is preferred as double vector type and the size of the population is given as 20. The population size is called as chromosome size. In addition, the creation function is elected as uniform. Then, the initial range is set as [100, 40, 50; 130, 70, 70] based on lowest and highest values of input variables. After completing the population phase, the fitness scaling type is given as rank type. Also, selection or reproduction type has been specified such as uniform and its elite count value is 2. In crossover function, single-point type is chosen and its crossover fraction value is 0.8. In mutation function, uniform type is selected and its rate is 0.01. In addition, plot function is termed as best fitness and best individual in the plot interval of 1. The migration direction is forward and its fraction and interval are 0.2 and 20, respectively. Initial penalty and its factor values are 10 and 100, respectively.

In stopping criteria, the generations values are set at 100 and stall generation value and stall limit time are 75 and 20, respectively. After setting all parameters, the solver has been run until the iteration is terminated. From this simulation, the optimized final results are obtained for those three variables which are shown in Table 6. In addition, the surface plots

Table 6
Optimized results

Variables	Venturi inlet length (a_v)	Venturi inlet width (b_v)	Cyclone outlet diameter (D_e)
Dimension (mm)	103.8	41.0	66.6

Table 5
ANOVA table for pressure drop

Source term	Degrees of freedom	Sequential sum of squares	Adjusted sum of squares	Adjusted mean squares	F Ratio	P Value
Regression model	9	438,143	438,143	48,682.6	769.57	0.000
Venturi inlet length (a_v)	1	34,766	166	166.4	2.63	0.166
Venturi inlet width (b_v)	1	158,599	1,767	1,766.7	27.93	0.003
Outlet diameter (D_e)	1	226,506	1,497	1,496.9	23.66	0.005
a_v^2	1	75	8	7.7	0.12	0.742
b_v^2	1	50	1	1.2	0.02	0.895
D_e^2	1	7,540	5,027	5,027.1	79.47	0.000
$a_v \times b_v$	1	1,187	1,187	1,187.0	18.76	0.007
$a_v \times D_e$	1	1,985	1,985	1,984.7	31.37	0.003
$b_v \times D_e$	1	7,435	7,435	7,435.2	117.54	0.000
Residual error	5	316	316	63.3		
Total	14	438,459				

such as generation vs. a fitness value and number of variables vs. current best individual values have been plotted as shown in Fig. 3. It is used to observe the best fitness value and mean of generations. The identified best fitness and mean fitness values are 266.2289 and 274.0084, respectively. The current best individual values of those three parameters are 103.8, 41 and 66.6, respectively. These optimized parameters are given less pressure drop and high collection efficiency compared with the mathematical model. This detail has been clearly discussed in comparison of the results section.

5. CFD analysis

In CFD, lots of turbulence models are obtainable to estimate the pressure drop, radial velocity, axial velocity and tangential velocity. Large Eddy simulations are problem contingent models. Furthermore, they are enormously related with geometries and boundary conditions of flow occupied [29]. Reynolds averaged Navier–Stokes equations have been employed to resolve when intricate geometric problems were concerned [13]. RSTM is regularly used to solve compound flow problems [9]. In this work, RSTM model has been used to simulate the Venturi inlet cyclone separator.

5.1. Mesh and boundary conditions

The mathematical and optimized Venturi inlet cyclone separator model has been created in SolidWorks software. Then, both models have been exported in IGS file format for mesh generation in Ansys Fluent software. The mesh has been generated for both mathematical and optimized cyclone separator by the finite volume method. The cut-cell type mesh model has been chosen for both models. Because the cut-cell type mesh is suitable for solving complex problems. The Lagrangian type reference frame choice has been set to these two models. In mesh sizing choice, smooth transition type has been mentioned. In addition, the growth rate and minimum edge length have been mentioned for both models such as 1 and 0.001 m respectively. The transition ratio is given as 0.272. The created nodes and elements for mathematical model are 219,623 and 187,802, respectively. The created nodes and elements for new model are 216,071 and 185,163, respectively. The created mesh worth has been validated in mesh metrics option by Ansys Fluent software. In this substantiation, the average skewness factor and aspect ratio have been accomplished as 0.03 and nearly equal to 1 correspondingly. It points out that the produced mesh has outstanding quality. In grid refinement test, three cases are considered for creating the mesh such as fine, medium and coarse type meshes. The grid refinement ratio has been predicted for both models of cyclone separator based on taking the ratio of total number of grids on fine mesh to total number of grids on medium mesh and total number of grids on medium type mesh to the total number of grids on coarse type mesh. The predicted grid refinement ratios for both models are 1.5 and 1.6, respectively. It indicates that the mesh quality is good because the refinement ratio is greater than the minimum value of 1.3. Moreover, this test confirms that the solution is not grid dependent. The inlet boundary condition has been preferred for the Venturi inlet is velocity. This state is applied to depict the velocity and scalar properties of stream. The proposed boundary condition for the outlet of the cyclone is pressure outlet. Further, no slip wall boundary condition has been preferred for entire walls of Venturi and cyclone separator. The meshed both cyclone separators are shown in Fig. 4. The mesh and boundary condition options are given in Table 7.

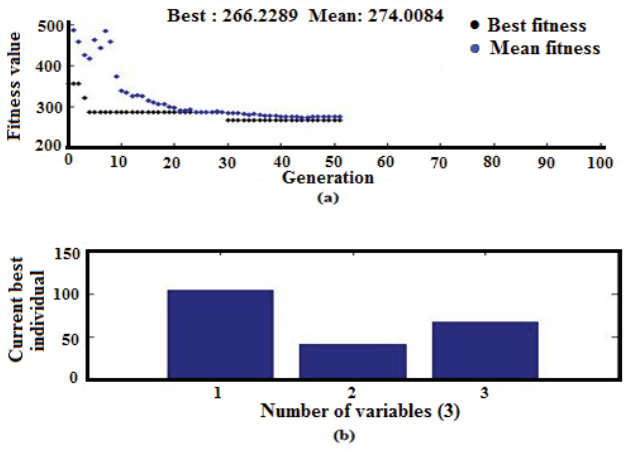

Fig. 3. (a) Generation vs. fitness value and (b) number of variables vs. current best individual.

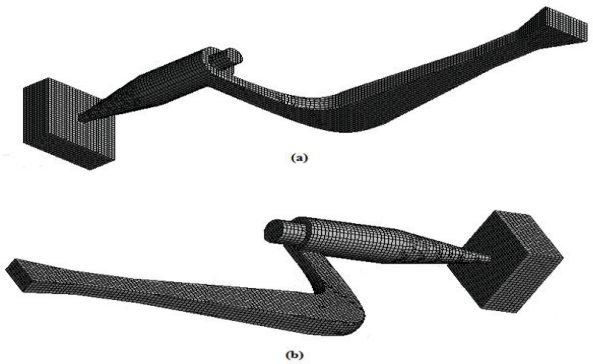

Fig. 4. Mesh for (a) mathematical model and (b) optimized model.

Table 7
Boundary conditions for mesh

S.No.	Cyclone model	Mesh type	Edge length (m)	No. of nodes	No. of elements	Boundary condition		
						Inlet	Outlet	Wall
1	Mathematical model	Cut-cell	0.001	219,623	187,802	Velocity inlet	Pressure outlet	No slip wall
2	New design	Cut-cell	0.001	216,071	185,163	Velocity inlet	Pressure outlet	No slip wall

5.2. Reynolds stress turbulence model

The RSTM is the most sophisticated turbulence model. In RSTM, for solving the 2D flows, five additional transport equations are needed. In addition, seven extra transport equations are needed to solve the 3D flows. The RSTM is a most suitable turbulence model for streamline curvature, swirl, rotation, and rapid changes in strain rate type problems compared with one equation and two equation models. It gives more accurate results for complex flows [30]. Due to this reason, in this study RSTM has been used for predicting pressure drop and particle tracking purpose.

5.3. Governing equations and solver settings

In this study, Ansys Fluent software (version 15) has been used for predicting the pressure drop and collection efficiency of the mathematical model and the new model cyclone separator. At first, the pressure-based velocity formulation has been preferred in solver type. Furthermore, transient flow has been preferred for this simulation. In viscous model panel, the Reynolds stress model has been selected. There are three subdivisions available such as a linear pressure-strain model, quadratic pressure-strain model and stress omega model. In this work, linear pressure-strain model has been chosen from the Reynolds stress type menu. In Fluent, the pressure-strain term is modelled from the exact transport equation according to the proposals given by Gibson and Launder [31] and Fu et al. [32]. The classical approach to modelling the φ_{ij} uses the following decomposition:

$$\phi_{ij} = \phi_{ij,1} + \phi_{ij,2} + \phi_{ij,\omega} \tag{10}$$

where $\varphi_{ij,1}$ is the slow pressure-strain term, $\varphi_{ij,2}$ is called the rapid pressure-strain term and $\varphi_{ij,\omega}$ is the wall-reaction term.

Equation for the slow pressure-strain term is as follows:

$$\phi_{ij,1} \equiv -C_1 \rho \frac{\in}{k}\left[\overline{u_i' u_j'} - \frac{2}{3}\delta_{ij} k\right] \tag{11}$$

where $C_1 = 1.8$.

Equation for the rapid pressure-strain term is as follows:

$$\phi_{ij,2} \equiv -C_2\left[\left(P_{ij} + F_{ij} + G_{ij} - C_{ij}\right) - \frac{2}{3}\delta_{ij}\left(P + G - C\right)\right] \tag{12}$$

where $C_2 = 0.60$, P_{ij} is stress production, F_{ij} is production by system rotation, G_{ij} is buoyancy production and C_{ij} is the convection. Also, where $P = \frac{1}{2}P_{kk}$, $G = \frac{1}{2}G_{kk}$ and $C = \frac{1}{2}C_{kk}$.

Moreover, the wall-reaction term, is responsible for the rescheduling of normal stresses near the wall. It leans to damp the normal stress perpendicular to the wall, while enhancing the stresses parallel to the wall. This term is modelled as follows:

$$\begin{aligned}\phi_{ij,w} \equiv C_1' \frac{\in}{k}\left(\overline{u_k' u_m'} n_k n_m \delta_{ij} - \frac{3}{2}\overline{u_i' u_k'} n_j n_k - \frac{3}{2}\overline{u_j' u_k'} n_i n_k\right)\frac{C_l k^{3/2}}{\in d} \\ + C_2'\left(\phi_{km,2} n_k n_m \delta_{ij} - \frac{3}{2}\phi_{ik,2} n_j n_k - \frac{3}{2}\phi_{jk,2} n_i n_k\right)\frac{C_l k^{3/2}}{\in d}\end{aligned} \tag{13}$$

where $C_1' = 0.5$, $C_2' = 0.3$, n_k is the x_k component of the unit normal to the wall, d is the normal distance to the wall and $C_l = C_\mu^{3/4}/k$, where $C_\mu = 0.09$ and k is the von Karman constant = 0.4187.

There are two alternatives available in Reynolds stress choices such as wall boundary condition from solving the k equation and wall reflection effects. First one is suitable for linear and quadratic pressure strain model and second one is suitable for linear pressure strain model. Moreover, four types are available in near wall treatment choice such as standard wall functions, scalable wall function, non-equilibrium wall function and enhanced wall treatment option. The standard wall function has been selected in this work. The standard wall functions have been mostly used for industrial flows [33]. They are provided as a default option in Fluent. The equation for this model is as follows:

$$U^* = \frac{1}{k}\ln\left(E_y^*\right) \tag{14}$$

where U^* is the mean velocity and y^* is the distance from wall and $E = 9.793$.

In boundary condition panel, at first the inlet velocity is specified as 5 m/s. Furthermore, intensity and hydraulic diameter values are given for the inlet and outlet boundary conditions. The turbulent intensity value for both mathematical and new model is 5%. The hydraulic diameter for mathematical model at the inlet port is 0.086 m and for the outlet is 0.050 m. The hydraulic diameter for new model at the inlet port is 0.059 m and for the outlet is 0.0666 m. No slip wall boundary condition has been preferred for the remaining walls of the Venturi cyclone, as the wall motion has been considered as stationary. The roughness constant has been set as 0.5. In solution method, SIMPLE scheme has been chosen for the pressure velocity coupling. Moreover, the least square cell-based option has been chosen in the spatial discretization. The momentum, turbulent kinetic energy and turbulent dissipation rate have been considered as second-order upwind from the discretization panel. The solution has been initialized by the hybrid initialization. The time step size and the number of time step have been specified as 0.001 and 4 s, respectively. In addition, utmost iterations for each time step have been given as 40. The static pressure contours, tangential, axial and radial velocity contours created subsequent to the solution has been converged.

5.4. Pressure contours

The contours of static pressure drop for mathematical model and optimized Venturi inlet cyclone separators are shown in Figs. 5 and 6. The predicted static pressure drop for mathematical model is 963.2 N/m^2 at velocity 5 m/s. For optimized design, it is 224 N/m^2. The contour plot depicts that the pressure is maximum at the Venturi inlet wall region, which is red in colour for both the mathematical and new designs. Moreover, the pressure is smallest amount at vortex finder and the outlet of cyclone separator which is blue in colour for the mathematical model and new model. Therefore, the pressure has been reduced from the Venturi inlet wall region to the outlet of cyclone separator. Further, the pressure is highest in cyclone separator cylinder wall region (green in colour)

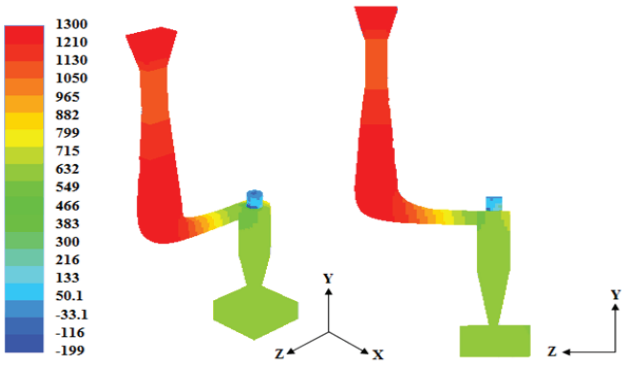

Fig. 5. Pressure contours for mathematical model.

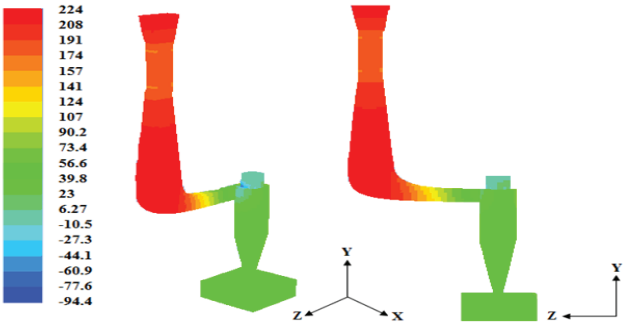

Fig. 6. Pressure contours for new design.

when compared with vortex finder region (blue in colour). This effect inveterate the particles are swirl within the cylinder wall section as a tropical storm and patch up at the underneath because the pressure is acute in cylinder wall area.

5.5. Velocity contours

The contours of radial, tangential and axial velocity of mathematical model Venturi inlet cyclone separator are shown in Fig. 7. The contour plot depicts that the maximum radial velocity is 31.5 m/s, tangential velocity is 18.2 m/s and the axial velocity is 16.1 m/s. Fig. 8 shows the contours of radial, tangential and axial velocity of new optimized design. From this contour plot, it is known that the maximum radial velocity is 14.1 m/s, tangential velocity is 4.57 m/s and the axial velocity is 5.6 m/s. The contour plots depict that the radial velocity is least in the Venturi inlet region and it reaches a maximum value at the vortex finder region for both designs. Furthermore, the tangential and axial velocity is least in inlet region and it reaches a maximum value around the vortex finder region. Also, these three velocities of the optimized model are very less compared with the mathematical model. Due to this reason, the particle escaping through the outlet port has been reduced in new model compared with the mathematical model. Fig. 9 illustrates the radial profile of calculated tangential and axial velocities for both cyclones at cylindrical section of the cyclone separator. This profile implies that the tangential velocity is least when compared with the mathematical model. As well, the axial velocity of novel design is a lesser amount when compared with the mathematical model (M letter shape). It denotes that

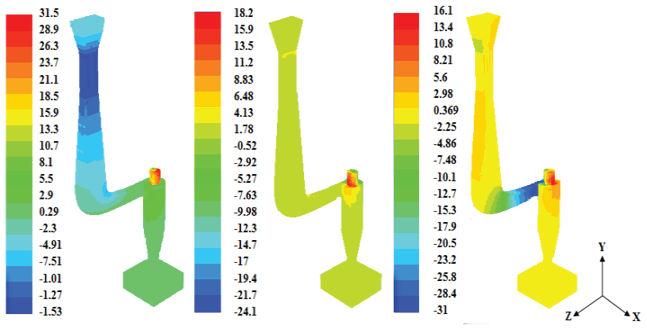

Fig. 7. Radial, tangential and axial velocity for mathematical model.

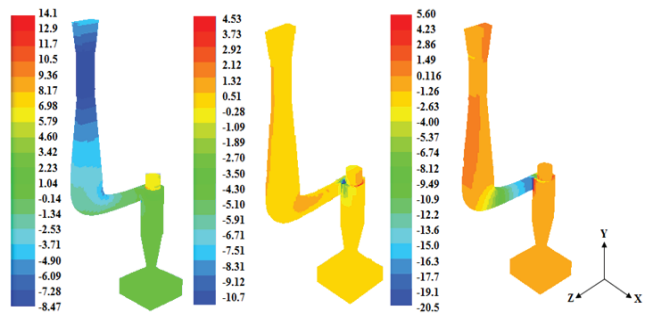

Fig. 8. Radial, tangential and axial velocity for new design.

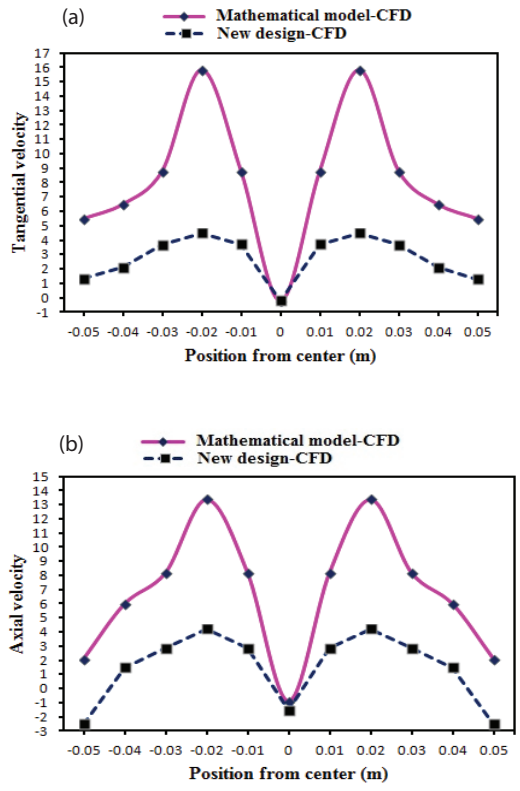

Fig. 9. Radial profile for calculated (a) tangential and (b) axial velocity.

the particle getaway through the outlet port has been diminished. It indicates that the collection efficiency of the new design is great. In addition, the radial profile demonstrates that the velocity is enlarged when the radial position is increased. After attaining its highest value, then it is reduced in the end section of the cylinder. Owing to these causes, the centrifugal force is initially increased. After attaining its highest value it is decreased. It means that the particles whirl within the cyclone similar to a tropical squall and settle at the base of the storage bin.

5.6. Discrete phase model

In Fluent, for estimating the cut-off diameter and collection efficiency of the cyclone separator, the DPM technique is used. The DPM follows Euler–Lagrange approach in Fluent. In this case, the fluid phase has been considered as a continuum by working out the time averaged Navier–Stokes equations even as the huge quantity of particles is in the path [34]. An important postulation has been considered in vanished phase as a small volume fraction which is 10%–12%. Furthermore, another important assumption is that continuation of particles does not influence the flow field, since a few particles merely hampered in cyclone separator [34]. Collisions between the particle and cyclone walls are taken as perfectly elastic. Therefore, the coefficient of restitution is equivalent to one. Moreover, the one-way coupling technique has been chosen for solving the equations of motion for particles. The equations of motion are as follows [35]:

$$\frac{\mathrm{d}u_p}{\mathrm{d}t} = F_D\left(u - u_p\right) + \frac{g_x(\rho_p - \rho)}{\rho_p} + F_x \tag{15}$$

$$F_D = \frac{18\mu}{\rho_p \mathrm{d}_p^2}\frac{C_D \mathrm{Re}}{24} \tag{16}$$

$$\mathrm{Re} = \frac{\rho \mathrm{d}_p \left|u_p - u\right|}{\mu} \tag{17}$$

In this study, spherical particle has been selected in drag law for describing the physical model in DPM. The drag coefficient, C_D, for spherical particle was found by correlations of Morsi and Alexander [36]. The drag coefficient is as follows:

$$C_D = a_1 + \frac{a_2}{\mathrm{Re}} + \frac{a_3}{\mathrm{Re}^2} \tag{18}$$

The dispersion of particles owing to turbulence in the fluid phase is computed by using the stochastic tracking model or the particle cloud model [33]. The stochastic tracking model has been chosen in this work. Also, this model uses the following equation to predict the turbulent dispersion of particles:

$$u = \overline{u} + u' \tag{19}$$

In addition, the discrete random walk (DRW) model has been preferred from stochastic tracking model to increase the number of particles injected through the inlet port of the Venturi. In this model, the eddy is characterized by Gaussian distributed random velocity and a time scale. The generalized Gaussian distribution for random velocity fluctuation and time scale equation for RSTM is as follows:

$$T_L \approx 0.30\frac{k}{\in} \tag{20}$$

$$\tau_e = 2T_L \tag{21}$$

where u is the fluid phase velocity, ρ_p is the density of the particle, F_x is an additional acceleration, ρ is the density of the fluid, the term $F_D(u - u_p)$ is drag force per unit particle mass, d_p is the particle diameter, u_p is the particle velocity, μ is the molecular viscosity of the fluid and Re is a relative Reynolds number, a_1, a_2 and a_3 are constants, $\overline{u}$ is the mean fluid phase velocity and u' is the random velocity [34].

5.6.1. Discrete phase model setting and results

The following boundaries have been set in DPM panel for computing the cut-off diameter and efficiency of the mathematical model and optimized model. The maximum number of steps and step length factor has been specified as 500,000 and 5, respectively, in the particle tracking panel. The injection type has been set as surface injection because the particles are released from the Venturi inlet surface. Moreover, the particle type is inert and the density of particle has been set as 2,000 kg/m^3. In addition, scale flow rate by face area and inject using face normal direction is chosen from injection panel. The flow rate and velocity have been set as 0.22 kg/s and 1 m/s, respectively, in point properties list. The spherical particle has been chosen in the drag law for describing the physical model. The distribution of particle diameter is preferred as uniform. The DRW model has preferred been from stochastic dispersion panel. The number of tries and time scale constant is set as 100 and 0.15 correspondingly. The efficiency has been estimated by number of particles introduced through the Venturi inlet, amount of particles runaway towards the outlet of cyclone and quantity of particles trapped in storage bin of the cyclone separator for various sizes of particle diameters. For estimating the collection efficiency, 2,600 particles were injected at a velocity of 1 m/s for mathematical model and 2,680 particles were injected for optimized new cyclone. The results are shown in Fig. 12. The graph has been plotted between particle diameters vs. efficiency of Venturi inlet cyclone. The efficiency of the optimized design is high when compared with mathematical model.

6. Comparison of results

The important geometric parameters of the Venturi inlet cyclone separator such as Venturi inlet length, Venturi inlet width and cyclone outlet diameter have been optimized by RSM and GA. The mathematical model and optimized new design variables are shown in Table 8. The result shows that the inlet length and width of the optimized dimensions are

less when compared with the mathematical model. Moreover, the exit diameter of the cyclone has increased when compared with mathematical model. The pressure drop, cut-off diameter, Euler number and Stokes number are calculated by these optimized results with the help of Eqs. (1), (3), (4) and Eq. (6), respectively. By these optimized results, the solid model has been created in modelling software then the same is analyzed in Ansys Fluent software for CFD analysis. Then, the mathematical and CFD results of the new design have been compared with each other.

Moreover, the mathematical and CFD results of the mathematical model have been compared with each other. The results are depicted in Table 9. The pressure drop and Euler number of the new model is 3.5 times less when compared with mathematical model. Also, the Stokes number and cut-off diameter of the new model is least when compared with the mathematical model. The efficiency of the new design is high when compared with mathematical model. In addition, the pressure drop has been estimated for the different inlet velocities (1–8 m/s) for both models. The results are depicted in Figs. 10 and 11. Further, the efficiency has been estimated for different sizes of the particle diameter for both models. The results are shown in Fig. 12. 100% of the particles are trapped in 26 μm of the particle diameter by mathematical model. 100% of the particles are trapped in 20 μm of the particle diameter by optimized new model. The efficiency of the new design and mathematical model has been compared by the CFD results with each other.

7. Conclusion

The important geometric parameters such as Venturi inlet length and Venturi inlet width and cyclone outlet diameter are related with Venturi inlet cyclone separator performance. The RSM and GA have been used to optimization. In addition, ANOVA has been used to estimate the significance of created quadric polynomial model from RSM. A good agreement has been obtained between RSM

Table 8
The modified new geometrical parameters and mathematical geometrical parameters

S.No.	Parameters	Mathematical model (m)	New design values (m)
1	Venturi inlet length (a_v)	0.125	0.1038
2	Venturi inlet width (b_v)	0.065	0.041
3	Cyclone outlet diameter (D_e)	0.050	0.0666

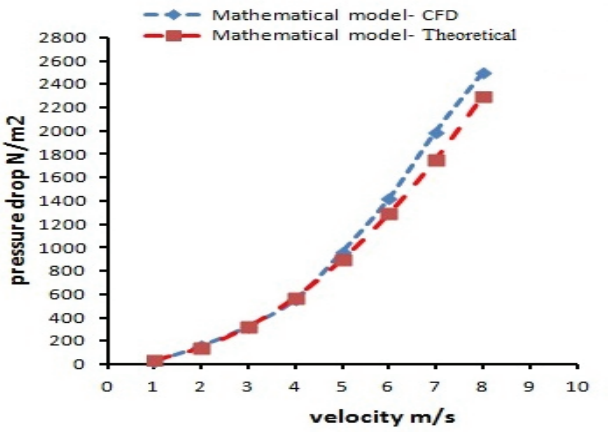

Fig. 10. Pressure drop at different velocities for mathematical model.

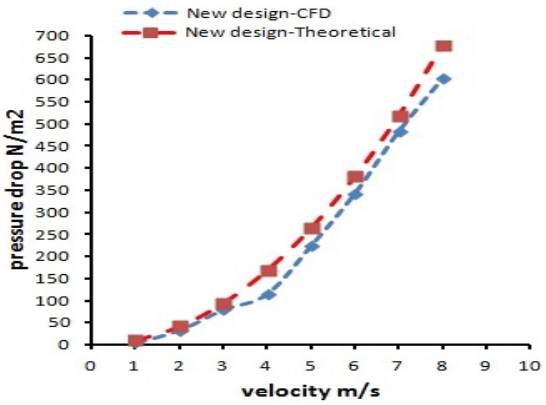

Fig. 11. Pressure drop at different velocities for new design.

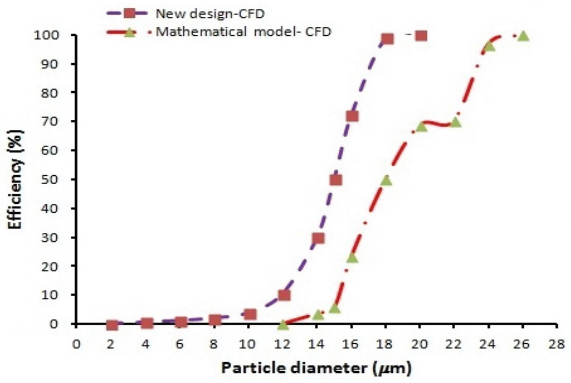

Fig. 12. Efficiency of both cyclones for different diameter of particles.

Table 9
Mathematical and CFD results for mathematical and new model

Method	Mathematical model				New model			
	Δp (N/m^2)	E_u	X_{50} (m)	Stk_{50}	Δp (N/m^2)	E_u	X_{50} (m)	Stk_{50}
Mathematical	895.8	58.54	1.85×10^{-5}	0.021364	264.5	17.28	1.47×10^{-5}	0.013448
CFD	963.3	62.95	1.87×10^{-5}	0.021828	224	14.64	1.52×10^{-5}	0.014422

and ANOVA results. This optimized new design gives less pressure drop and high collection efficiency. Moreover, the cut-off diameter, Euler number and Stokes number of the new design are less when compared with mathematical model. From this optimized result one can conclude that decreasing the inlet length and inlet width and increasing the outlet diameter produce less pressure drop and high collection efficiency. The factor pressure drop is directly proportional to head. The parameter head is directly proportional to Venturi inlet length and width, whereas indirectly proportional to the outlet diameter. Therefore, variations in the pressure drop can only be attained through varying the head. Decreasing the inlet length and inlet width and increasing the outlet diameter produce less head. Due to this less head, the pressure drop between the inlet and outlet port has been reduced. Moreover, travelling speed of the particle is reduced due to this less pressure drop. Therefore, the particles escaping through the outlet tube has been reduced. It means most of the particles are trapped in the collecting bin. It confirms that the collection efficiency of optimized model is maximum. The RSTM and DPM are most suitable CFD techniques to predict the pressure drop, cut-off diameter, Euler number and Stokes number. A good agreement has been obtained between mathematical and CFD results. Moreover, the radial profiles for the tangential and axial velocities of both designs imply that the collection efficiency of the new design is high when compared with mathematical model. In addition, one can conclude that this optimized model consumes less energy and collects more particles compared with mathematical model due to less pressure drop. Further, it reduces the environmental impact and reduces the energy consumption of secondary purification processes because of high collection efficiency of this optimized equipment.

Acknowledgements

The authors would like to thank Dr. Malathi, Professor, EASA College of Engineering and technology for language editing and the authors also thank Avinashilingam, Gopalsamy, Arulkumar and Hariprasath (Sri Eshwar College of Engineering) for technical support in this research.

Symbols

D_e	—	Outlet diameter, m
S	—	Outlet length, m
a	—	Inlet height, m
h	—	Body height, m
H_t	—	Total height, m
D	—	Cyclone cylinder diameter, m
B_c	—	Cone tip diameter, m
b	—	Inlet width, m
a_v	—	Venturi inlet length, m
b_v	—	Venturi inlet width, m
h_c	—	Height of convergent section, m
h_d	—	Height of divergent section, m
h_t	—	Height of throat section, m
a_t	—	Venturi throat length, m
b_t	—	Venturi throat width, m
H_v	—	Total height of the Venturi, m
Δp	—	Pressure drop, N/m^2
ρ_p, ρ_g	—	Particle density, fluid or gas density, kg/m^3
V_i	—	Inlet velocity, m/s
Stk_{50}	—	Stokes number
β_o, β_i, β_{ii}, β_{ij}	—	Regression coefficients for intercept, linear, quadratic and interaction terms
X_i, X_j	—	Independent variables
Y	—	Response variables
H_d	—	Head
X_{50}	—	Cut-off diameter of the particle, m
E_u	—	Euler number
μ	—	Fluid viscosity, kg/ms
N_e	—	Number of turns
$\varphi_{ij,}$ $\varphi_{ij,1,}$ $\varphi_{ij,2,}$ $\varphi_{ij,\omega}$	—	Pressure strain, slow pressure strain, rapid pressure strain, wall reaction term
$C_1, C_2, C_1', C_2', C_1 \ldots$	—	Model constants
k	—	Turbulent kinetic energy, m^2/s^2
$\in$	—	Turbulent kinetic dissipation rate, m^2/s^3
T	—	Time, s
$\overline{u_i'u_j'}$	—	Reynolds stress tensor
δ_{ij}	—	Boundary layer thickness
P_{ij}	—	Stress production
F_{ij}	—	Production by system rotation
G_{ij}	—	Buoyancy production
C_{ij}	—	Convection
n_i, n_j, n_k	—	Unit normal to the wall
U^*, y^*	—	Mean velocity, m/s, distance from wall, m
u_i, u_j, u_k	—	Velocity component in corresponding direction, m/s
μ_t	—	Turbulence viscosity, Pa s
u_p	—	Particle velocity, m/s
U	—	Fluid phase velocity, m/s
F_D	—	Drag force, N
F_X	—	Additional force, N
d_p	—	Particle diameter, m
Re	—	Relative Reynolds number
C_D	—	Drag coefficient of particle
$\overline{u}$	—	Mean fluid phase velocity, m/s
u'	—	Random velocity fluctuation, m/s
a_1, a_2, a_3	—	Constants
T_L	—	Fluid Lagrangian integral time, s
τ_e	—	Time scale, s

Reference

[1] H. Xu, J. Liu, Y. Wang, G. Cheng, X. Deng, X. Li, Oil removing efficiency in oil-water separation flotation column, Desal. Wat. Treat., 53 (2015) 2456–2463.

[2] F. Boysan, W.H. Ayers, J. Swithenbank, A fundamental mathematical modelling approach to cyclone design, Trans. Inst. Chem. Eng., 60 (1982) 222–230.

[3] J.H. Son, M. Hong, H.C. Yoo, Y.I. Kim, H.D. Kim, J.T. Kim, A multi-hydro cyclone water pretreatment system to reduce suspended solids and the chemical oxygen demand, Desal. Wat. Treat., 57 (2016) 2996–3001.

[4] W. Xu, Q. Li, J. Wang, Y. Jin, Performance evaluation of a new cyclone separator – part II simulation results, Sep. Purif. Technol., 160 (2016) 112–116.
[5] X. Gu, J. Song, Y. Wei, Experimental study of pressure fluctuation in a gas-solid cyclone separator, Powder Technol., 299 (2016) 217–225.
[6] K. Elsayed, C. Lacor, The effect of the dust outlet geometry on the performance and hydrodynamics of gas cyclones, Comput. Fluids, 68 (2012) 134–147.
[7] Y. Su, A. Zheng, B. Zhao, Numerical simulation of effect of inlet configuration on square cyclone separator performance, Powder Technol., 210 (2011) 293–303.
[8] S. Bernardo, M. Mori, A.P. Peres, R.P. Dionisio, 3-D computational fluid dynamics for gas and gas particle flows in a cyclone with different inlet section angles, Powder Technol., 162 (2006) 190–200.
[9] J. Gimbun, T.G. Chuah, T.S.Y. Choong, A. Fakhru'l-Razi, Prediction of the effects of cone tip diameter on the cyclone performance, J. Aerosol Sci., 36 (2005) 1056–1065.
[10] J. Chen, X. Liu, Simulation of a modified cyclone separator with a novel exhaust, Sep. Purif. Technol., 73 (2010) 100–105.
[11] G. Gong, Z. Yang, S. Zhu, Numerical simulation of the effect of helix angle and leaf margin on the flow pattern and the performance of the axial flow cyclone separator, Appl. Math. Modell., 36 (2012) 3916–3930.
[12] A. Raoufi, M. Shams, M. Farzaneh, R. Ebrahimi, Numerical simulation and optimization of fluid flow in cyclone vortex finder, Chem. Eng. Process., 47 (2008) 128–137.
[13] H. Safikhani, M.A. Akhavan-Behabadi, N. Nariman-Zadeh, M.J. Mahmood Abadi, Modeling and multi-objective optimization of square cyclones using CFD and neural networks, Chem. Eng. Res. Des., 89 (2011) 301–309.
[14] S. Pishbin, M. Moghiman, Optimization of cyclone separators using genetic algorithm, Chem. Eng., 2 (2010) 686–691.
[15] M.B. Ray, P.E. Luning, A.C. Hoffmann, Post cyclone (PoC): an innovative way to reduce the emission of fines from industrial cyclones, Ind. Eng. Chem. Res., 36 (1997) 2766–2774.
[16] J. Jiao, Y. Zheng, G. Sun, J. Wang, Study of the separation efficiency and flow field of a dynamic cyclone, Sep. Purif. Technol., 49 (2006) 157–166.
[17] C.J. Stairmand, The design and performance of cyclone separators, Ind. Eng. Chem., 29 (1951) 356–383.
[18] A. Avci, I. Karagoz, Theoretical investigation of pressure losses in cyclone separators, Int. Commun. Heat Mass Transfer, 28 (2001) 107–117.
[19] E. Muschelknautz, M. Trefz, Design and Calculation of Higher and Highest Loaded Gas Cyclones, Proceedings of Second World Congress on Particle Technology, 1990, pp. 52–71.
[20] J. Chen, M. Shi, A universal model to calculate cyclone pressure drop, Powder Technol., 171 (2007) 184–191.
[21] B. Zhao, A theoretical approach to pressure drop across cyclone separators, Chem. Eng. Technol., 27 (2004) 1105–1108.
[22] C.B. Shepherd, C.E. Lapple, Flow pattern and pressure drop in cyclone dust collectors, Ind. Eng. Chem., 31 (1939) 972–984.
[23] R.K. Sinnott, Chemical Engineering Design, Elsevier Science, Oxford, 2005.
[24] K. Elsayed, C. Lacor, Optimization of the cyclone separator geometry for minimum pressure drop using mathematical models and CFD simulations, Chem. Eng. Sci., 65 (2010) 6048–6058.
[25] J.S. Cowpe, J.S. Astin, R.D. Pilkington, A.E. Hill, Application of response surface methodology to laser-induced breakdown spectroscopy: influences of hardware configuration, Spectrochim. Acta, Part B, 62 (2007) 1335–1342.
[26] G.E.P. Box, K.B. Wilson, On the experimental attainment of optimum conditions, J. R. Stat. Soc., 13 (1951) 1–45.
[27] Z. Michalevicz, Genetic Algorithms + Data Structures = Evolution Programs, Springer, New York, 1992.
[28] C.R. Reeves, Genetic algorithms for the operation researcher, INFORMS J. Comput., 9 (1997) 231–250.
[29] G. Gronald, J.J. Derksen, Simulating turbulent swirling flow in a gas cyclone: a comparison of various modeling approaches, Powder Technol., 205 (2011) 160–171.
[30] B.E. Launder, N. Shima, Second-moment closure for the near-wall sub layer: development and application, AIAA J., 27 (1989) 1319–1325.
[31] M.M. Gibson, B.E. Launder, Ground effects on pressure fluctuations in the atmospheric boundary layer, J. Fluid Mech., 86 (1978) 491–511.
[32] S. Fu, B.E. Launder, M.A. Leschziner, Modeling Strongly Swirling Recirculating Jet Flow with Reynolds-Stress Transport Closures, Sixth Symposium on Turbulent Shear Flows, Toulouse, France, 1987.
[33] B.E. Launder, D.B. Spalding, The numerical computation of turbulent flows, Comput. Methods Appl. Mech. Eng., 3 (1974) 269–289.
[34] Fluent, Inc., Fluent 6.1.22 Users' Guide, 2004.
[35] B. Zhao, Y. Su, J. Zhang, Simulation of gas flow pattern and separation efficiency in cyclone with conventional single and spiral double inlet configuration, Chem. Eng. Res. Des., 84 (2006) 1158–1165.
[36] S.A. Morsi, A.J. Alexander, An investigation of particle trajectories in two phase flow systems, J. Fluid Mech., 55 (1972) 193–208.